HHS Public Access

Author manuscript

Chemistry. Author manuscript; available in PMC 2016 March 21.

Published in final edited form as:

Chemistry. 2015 January 19; 21(4): 1673–1681. doi:10.1002/chem.201405176.

Acid-base triggered switching of circularly polarized luminescence and electronic circular dichroism in organic and organometallic helicenes

Nidal Saleh[a], **Barry Moore II**[b], **Monika Srebro**[c], **Nicolas Vanthuyne**[d], **Loïc Toupet**[a], **J. A. Gareth Williams**[e], **Christian Roussel**[d], **Kirandeep K. Deol**[f], **Gilles Muller**[f], **Jochen Autschbach**[b], and **Jeanne Crassous**[a]

Jochen Autschbach: jochena@buffalo.edu.; Jeanne Crassous: jeanne.crassous@univ-rennes1.fr

[a]Institut des Sciences Chimiques de Rennes, UMR 6226, Institut de Physique de Rennes, UMR 6251, Campus de Beaulieu, CNRS-Université de Rennes 1, 35042 Rennes Cedex, France [b]Department of Chemistry, University at Buffalo, State University of New York, Buffalo, NY 14260, USA [c]Faculty of Chemistry, Jagiellonian University, 30-060 Krakow, Poland [d]Aix Marseille Université, Centrale Marseille, CNRS, iSm2 UMR 7313, 13397, Marseille, France [e]Department of Chemistry, University of Durham, Durham, DH1 3LE, UK [f]Department of Chemistry, San José State University, San José, CA 95192-0101, USA

Abstract

Electronic circular dichroism and circularly polarized luminescence acid-base switching activity is demonstrated in helicene-bipyridine proligand (**1a**) and in its “rollover” cycloplatinated derivative (**2a**). While proligand **1a** displays a strong bathochromic shift (>160 nm) of the non polarized and circularly luminescence upon protonation, complex **2a** displays slightly stronger emission. This striking different behavior between singlet emission in the organic helicene and triplet emission in the organometallic one is rationalized using theory. The very large bathochromic shift of the emission observed upon protonation of azahelicene-bipyridine **1a** was rationalized by the decrease of aromaticity (promoting a charge transfer-type transition rather than a π–π* one) along with an increase of the HOMO-LUMO character of the transition and stabilization of the LUMO level upon protonation.

Graphical abstract

Correspondence to: Jochen Autschbach, jochena@buffalo.edu.; Jeanne Crassous, jeanne.crassous@univ-rennes1.fr.

Supplementary information for this article is given via a link at the end of the document.

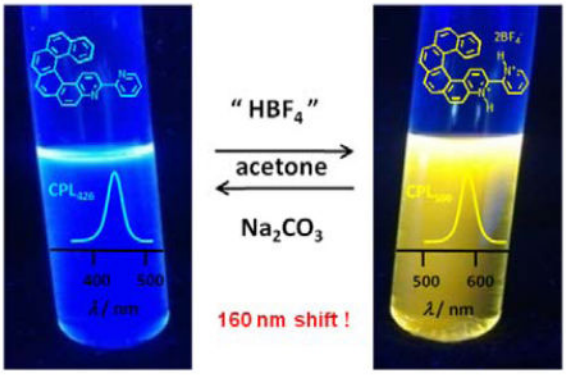

A [6]Helicene-bipyridine derivative is used as a proligand for “rollover” cycloplatination and for the conception of acid-base chiroptical switches. The protonation triggers the nature of the HOMO-LUMO transition, from a π–π* type to a charge transfer one and significantly modifies the circularly polarized luminescence and electronic circular dichroism spectra of organic and organometallic helicenes

Keywords

helicene; 2,2′-bipyridine; chiroptical switch; CPL; time-dependent density functional theory

Introduction

The development of chiral molecules displaying large chiroptical properties may lead to novel multifunctional molecular materials.[1] In this area, helicenes show great potential. Due to their π-conjugated helical backbone, they combine high optical activity with other properties such as intense emission.[2,3] Recently, organometallic helicenes in which a transition metal (Pt, Ir, Os) is included within the helical π-framework have emerged as promising candidates for opto-electronic applications and as good chiral emitters.[3e,4] Devices displaying circularly polarized luminescence (CPL) are of great interest since CPL activity may be a powerful method to address encoded information (cryptography) or for 3D displays.[5a] More generally, systems that possess switchable CPL functionality may lead to new possibilities for molecular information processing and storage.[5b]

In this paper, we describe the regioselective rollover cycloplatination of a helicene-2,2′-bipyridine proligand,[6] namely 3-(2-pyridyl)-4-aza[6]helicene (**1a**), Scheme 1. The new organic and organometallic helicene derivatives act as unprecedented multifunctional pH-switchable chemical systems due to the reversible tuning of their optical and chiroptical properties: optical rotation (OR), electronic circular dichroism (ECD), non-polarized luminescence and CPL. The different behaviors of these ECD and CPL switches are interpreted based on results from first-principles calculations.

Results and Discussion

The synthesis of racemic 3-(2-pyridyl)-4-aza[6]helicene **1a** was performed in two steps from 2,2′-bipyridine-6-carboxaldehyde, by a Wittig reaction with 2-methylbenzophenanthrene phosphonium bromide[7] followed by a photocyclization reaction (83% overall yield),[2] and enantiopure *M*- and *P*-**1a** (*ee*'s >99%) were subsequently obtained by HPLC over a Chiralpak IC stationary phase (see Supporting Information, SI). 3-(2-Pyridyl)-4-aza[6]helicene (**1a**) has been fully characterized and displays classical spectrocopic features of helicenes (see Experimental Part). The X-ray crystallographic structure of a smaller model molecule, *i.e.* 3-(2-pyridyl)-4-aza[4]helicene **1b** displayed in Scheme 2 shows *i*) the helical aza[4]helicene part (helicity 25.13°), *ii*) the grafted 2-pyridyl group which is coplanar with the helicene part (dihedral angles of −1.17 and 5.35 between the two pyridyl rings) and *iii*) the two nitrogen atoms in mutually *trans* positions.

Examples of molecular materials based on chiral bipy ligands and their complexes are still rare.[8] Apart from their common 1,4-*N*,*N*′ chelating behavior, 2,2′-bipyridines can act as 1,4-*C*,*N* chelates through the direct metal-mediated C-H bond activation at the 3-position of the 2-pyridyl ring and undergo the so-called "rollover" cyclometalation.[9,10] The $N^{1'}$-C^2 rollover cycloplatination of *M*- and *P*-**1a** to enantiopure complexes *M*- and *P*-**2a** (Scheme 1) was performed by reacting respectively *M*- and *P*-**1a** with electron-rich $[Pt(dmso)_2(CH_3)_2]$ precursor at 50°C in acetone for 5 hours (87% yield). The formation, regioselectivity, and stereochemistry of the neutral square-planar Pt(II) complex **2a** was established by multinuclear NMR spectroscopy. For example, the ^{1}H NMR spectrum at 400 MHz revealed the disappearance of the H^2 signal, the strong deshielding (1 ppm) of proton $H^{6'}$ (9.5 ppm) with satellites due to a $^3J(^{195}Pt, ^1H)$ coupling constant of 20 Hz, and the H^1 proton appearing at 8.1 ppm with a $^3J(^{195}Pt, ^1H)$ of 63 Hz, all confirming the C^2–Pt and $N^{1'}$–Pt bond formation. These results show that the CH activation process proceeded regioselectively at the C^2 position only.[10] Due to *trans* effects, the cycloplatination is also stereoselective, with the dmso *S*-ligand placed *trans* to the C^2 carbon. Note that the Pt–CH_3 signal appears at −0.34 ppm ($^2J(^{195}Pt, ^1H)$ = 83 Hz) while the two dmso methyl groups are diastereotopic with the $^3J(^{195}Pt, ^1H)$ coupling constant (18 Hz).[10] Using the same conditions as for **2a**, the regio- and stereoselective $N^{1'}$-C^2 rollover cycloplatination of model proligand **1b** gave complex **2b** with 89% yield (Scheme 2). This compound displayed the same spectroscopic features as **2a**. Furthermore, reaction of complex **2b** with HCl (0.1N) followed by reaction with triphenylphosphine, yielded complex **3b** in which the PPh_3 ligand is *trans* to the $N^{1'}$ nitrogen and a chlorine is placed *trans* to the C^2 carbon.[10d] The X-ray crystallographic structure of **3b** finally ascertained the presence of the platinacycle (Scheme 2).[11] Noteworthy, very low dihedral angles (2–3°) between the two pyridyl rings ensure that the π-conjugation extends across the whole molecule. The N atom of the helical moiety remains free for protonation (*vide infra*).[10e]

Azahelicenes are known to exhibit high proton affinities[12] and some of them behave as proton sponges,[12b] while, according to Zucca *et al.*, in the protonated rollover cycloplatinated complex the ligand may be considered as an "abnormal remote heterocyclic chelated carbene or simply as mesoionic cyclometalated ligand".[10e] Therefore, in our quest for original new organometallic helicene-based chiroptical switches,[13a,14] we investigated

the acid-base reactivity and the use of organic helicene **1a** and cycloplatinated helicene **2a** as potential multifunctional pH-triggered UV-vis, OR, ECD and/or CPL switches. The acid $[H_2O.HBF_4]_2$[18C6] ("HBF_4")[10d,15] in acetone or CH_2Cl_2 was used to protonate either proligand **1a** or rollover complex **2a** into respectively *M*-(−) and *P*-(+) enantiopure forms of [**1a**,$2H^+$][$2BF_4^-$] and [**2a**,H^+][BF_4^-] while treatment with Na_2CO_3 or NEt_3 enabled the recovery of the neutral forms (Scheme 1). The unusual electronic properties of these systems were rationalized with the help of density functional theory (DFT) and time-dependent DFT, using the BHLYP functional (50% exact exchange) and a split-valence basis with polarization functions for non-hydrogen atoms (SV(P)) for most calculations. Computational details, detailed analyses, and additional results not discussed herein, are provided in the Supplementary Information (SI).

The UV-vis absorption spectrum of **1a** (SI) is typical of an extended π-conjugated system, with a strong band ($\varepsilon > 50\times10^3$ M^{-1} cm^{-1}) at 266 nm, and several structured broad bands around 330, 350 and 393 nm. Proligand *P*-**1a** displays a strong, structured, negative CD band at c.a. 264 nm ($\Delta\varepsilon = -183$ $M^{-1}cm^{-1}$) and strong positive bands at 333, 352 and 375 nm ($\Delta\varepsilon = +235, +107, +42$ $M^{-1}cm^{-1}$), Figure 1. These values are stronger than for unsubstituted 4-aza[6]helicene,[13] owing to the extended π-conjugation and partial charge transfer (CT) character of the lowest-energy π–π* excitations (dominantly from the highest occupied molecular orbital (HOMO, H, Figure 3) to the lowest unoccupied MO (LUMO,L). A high molar rotation is observed for **1a** (*P*-**1a**: $[\varphi]_D = +12000 \circ cm^2$ $dmol^{-1}$ (±5%), in CH_2Cl_2, 6.5×10^{-5} M, calc. BHLYP +14176).

Proligand **1a** exhibits emission behavior typical of π-conjugated polyaromatic hydrocarbons and previously described helicenes.[2,3,13c] In CH_2Cl_2 solution at r.t., **1a** displays classical structured blue fluorescence with a maximum ($\lambda_{0\text{-}0}$) at 421 nm and a vibronic progression of 1400 cm^{-1} (quantum yield Φ 8.4% and fluorescence lifetime τ 6.6 ns, see Figure 2 and Figure S16; emission data for all compounds are summarized in Tables 1 and S3). A particularly interesting feature of fluorescent derivatives *P*-(+) and *M*-(−)-**1a** is that they exhibit CPL (Figures 2a)[3] with mirror-imaged spectra and respective luminescence dissymmetry ratios g_{lum} of $+3.4\times10^{-3}$ and -3×10^{-3} around the emission maximum (426 nm). These g_{lum} values are comparable to other fluorescent organic azahelicene derivatives.[3]

The UV-vis spectrum of **2a** shows a similar shape as **1a** and has a similar helicene-centered assignment. The CD spectrum of *P*-**2a** (Figure 1) displays two strong negative bands at 264 and 287 nm ($\Delta\varepsilon = -131, -130$ $M^{-1}cm^{-1}$) and several strong to moderate positive bands at 343, 386, 403, 429 nm ($\Delta\varepsilon$= 212, 73, 41, 23 $M^{-1}cm^{-1}$) that are ~10 nm red-shifted compared to *P*-**1a** with the lower-energy π–π* excitations exhibiting significant intra-ligand charge transfer (ILCT) character. The MOs involved in the lower-energy excitations do not indicate a strong involvement of Pt 5*d* orbitals. The metal's dominant role is to render the structure of the chromophore rigid and to promotes intersystem crossing (*vide infra*). A high molar rotation value is observed for **2a** (*P*-**2a**: $[\varphi]_D = +18730$ (±5%), in CH_2Cl_2, 7×10^{-5} M, calc. BHLYP +19345). In contrast to **1a**, the rollover cycloplatinated helicene **2a** displays red phosphorescence at r.t. (λ_{max} = 547 nm, Φ = 0.3%, τ = 8.2 μs), with no fluorescence band (Figures 2 and S18, Tables 1 and S3). Such behaviour is expected for cycloplatinated

complexes due to strong spin-orbit coupling. The low quantum yield and estimated radiative rate constant of around 200 s^{-1} suggest that the phosphorescence is relatively inefficient, reflecting the decreasing contribution of the metal to the excited state, in agreement with the calculations. Phosphorescent derivatives *P*-(+) and *M*-(−)-**2a** are CPL active (Figure 2b),[3] and display mirror-imaged CPL spectra with g_{lum} values of $+1\times10^{-3}$ and -1.1×10^{-3} around the emission maximum (547 nm). These values are lower than those of previously published platina[6]helicenes ($g_{lum}\sim10^{-2}$),[3e] because the Pt center is less involved in the helical π-core of the molecule, as indicated by the calculations.[5c-f]

Upon protonation by an excess of "HBF_4" in acetone, *P*-[**2a**,H^+][BF_4^-] and *M*-[**2a**,H^+][BF_4^-] were obtained quantitatively within two hours (Scheme 1). Their ^1H NMR spectra displayed overall downfield shifted signals and the appearance of the NH^+ signal at 13.5 ppm (SI). Interestingly, the UV-vis spectra of protonated complexes *P*-[**2a**,H^+][BF_4^-] and *M*-[**2a**,H^+][BF_4^-] were significantly different from the non-protonated *P*-and *M*-**2a**, with a stronger broad band at longer wavelengths (380–510 nm, λ_{max} = 467 nm, ε = 8260 $M^{-1}cm^{-1}$, Figure S9) than the corresponding neutral species (380–460 nm, λ_{max} = 429 nm, ε = 5800 $M^{-1}cm^{-1}$). Similarly, ECD spectra were substantially modified, with ~10 nm red-shifted negative bands at 273 and 293 nm ($\Delta\varepsilon$ = −116, −86 $M^{-1}cm^{-1}$), a less intense positive band at 345 nm ($\Delta\varepsilon$ = +135 $M^{-1}cm^{-1}$), and strong band at 465 nm ($\Delta\varepsilon$ = +34 $M^{-1}cm^{-1}$) for the *P*-[**2a**,H^+][BF_4^-] enantiomer (Figure 1). Note that several isosbestic points are appearing in the UV-vis and CD spectra upon successive addition of 0.1 eq of "HBF_4" (see Figures S9 and S11). The protonation of enantiopure *M*- and *P*-proligands **1a** was also performed under the same conditions, i.e. by reacting with a slight excess of "HBF_4" in either acetone or CH_2Cl_2 thus yielding *M*- and *P*-[**1a**,$2H^+$][$2BF_4^-$] quantitatively. The ^1H NMR spectrum displayes downfield shifts of all the signals, i.e. aza[6]helicene and pyridyl moiety (for example $\Delta\delta$ = 0.6 and 0.2 ppm for $H^{6'}$ and H^{15} respectively), consistent with the presence of two NH^+.

Compared to **1a**, the UV-vis spectrum of protonated [**1a**,$2H^+$][$2BF_4^-$] displays a new low-energy band of moderate intensity (ε = 3500 $M^{-1}cm^{-1}$, Figure S8) between 430 and 530 nm and is slightly different in the 250–350 nm region. The ECD-active bands in the 250–350 nm region are significantly lowered (for example $\Delta\varepsilon$ = +44 *vs.* 111 $M^{-1}cm^{-1}$ at 348 nm for *P*-[**1a**,$2H^+$][$2BF_4^-$] and *P*-**1a**, respectively) while a new ECD-active band has appeared around 430–530 nm ($\Delta\varepsilon$ = +14 $M^{-1}cm^{-1}$ at 430 nm), Figure 1.[12a] The UV-vis and CD spectra are accompanied with the appearance of several isosbestic points upon successive addition of 0.1 eq of "HBF_4" (see Figures S8 and S10). However, it was not possible to identify a mono-protonated intermediate, which suggests that both pyridyl cycles undergo protonation simultaneously. Intramolecular proton transfer between the two pyridyls may also occur.[12d] Note that the charged protonated systems are very challenging for the calculations due to solvent- [12a] and counter-ion – effects (see SI). However, the most important trends upon protonation observed experimentally are correctly reproduced by the calculations, in particular the appearance of low-energy absorption and ECD bands. Protonation has a strong effect on the delocalization of the extended π-systems of both **1a** and **2a**. For instance, the new lowest-energy ECD band in [**2a**,H^+] is assigned as dominantly H-L π–π^* similar to **2a**, but unlike **2a** the transition is now a much more clear-cut CT case

from the helicene moiety to the other side of the ligand. The frontier MOs of **2a** are conjugated through the pyridyl, but upon protonation the orbitals become spatially separated as demonstrated in Figure 1. Nucleus-independent chemical shift calculations for a model system as described in the SI suggest that the pyridyl becomes less aromatic upon protonation. Therefore, we attribute the increase in CT character to a loss of conjugation of the frontier orbitals caused by a reduction of aromatic character in the pyridyl moiety. The overall contribution of the H-L pair to the transition increases upon protonation, which further amplifies the increase of CT character (Table 2). Similar changes upon protonation can be observed for **1a**. The S_0–S_1 absorption becomes even more purely of H-L character here. Inspection of the orbital energies (Table S7) shows that protonation has a strongly stabilizing effect on the LUMO of **2a** and even more so on **1a**, and to a much lesser extent on the HOMO, reducing the H-L gap. The frontier MOs calculated for both **1a** and **2a** appear very similar (Figure 3). All exhibit large values of the LUMOs around the pendant pyridyl nitrogen while the HOMOs have nodes at this position. The same was found for MOs at the S_1 and T_1 optimized geometries (Figure S33, *vide infra*). Therefore, the appearance of the low-energy ECD bands upon protonation of both systems can be rationalized mainly by its impact on the LUMO and simultaneously the S_0–S_1 transition becoming more dominant in H-L character. The protonation has also an effect on the optical rotation. Molar rotations appeared lower for bis-protonated *P*-[**1a**,$2H^+$][$2BF_4^-$] ($[\varphi]_D$ = +10000 (±5%), in CH_2Cl_2, 1.7×10^{-4} M) than for *P*-**1a**, and decreased even more for the protonated complex *P*-[**2a**,H^+][BF_4^-] ($[\varphi]_D$ = +9145 (±5%), CH_2Cl_2, 1.5×10^{-5} M). Calculations (Table S4) indicate that the counterion(s) may play a role in these strong reductions. Furthermore, as depicted in Figure 4, successive addition of "HBF_4" and NEt_3 in either acetone or CH_2Cl_2 to 3-(2-pyridyl)-4-aza[6]helicene (**1a**) and its cycloplatinated complex 2a enabled reversible and repeatable modification of the OR and ECD values, and hence the system constitutes a pH-triggered chiroptical switch.

The luminescence λ_{max} of **2a** undergoes much less of a change upon protonation than its ECD or the ECD and CPL of **1a** (Figure 2b). The calculated T_1–S_0 emission energies are likewise very similar for **2a** and its protonated form (Table 1) and in good agreement with experiment. Only for this transition we found a decrease of H-L character upon protonation which renders the reduction of the H-L orbital energy gap due to protonation less important (Table 1), leading to a decrease of the calculated emission energy by only 0.1 eV. The estimated radiative rate constant remains around 200 s^{-1}, but the phosphorescence quantum yield is larger and the lifetime longer (λ_{max} = 555, 590 nm, Φ = 2.7%, τ = 120 μs), suggesting that non-radiative decay pathways are impeded in the protonated form. The CPL activity is doubled in the protonated species (g_{lum}= $+1.8\times10^{-3}$ and -2.2×10^{-3} for *P*- and *M*-[**2a**,H^+][BF_4^-] respectively, Figure 2b).

Helicene **1a** shows a more striking change in its luminescence upon protonation. The emission is strongly bathochromically shifted, from λ_{max} = 426 nm in **1a** to 590 nm in [**1a**, $2H^+$][$2BF_4^-$] (a shift of −0.8 eV, in CH_2Cl_2 solution at r.t., Figure 2a, Table S3). The calculations also produce a large bathochromic shift (−1.1 eV) for the S_1-S_0 emission upon protonation of **1a**, Table S8, mirroring a similar shift in the calculated S_0-S_1 excitation energies. The S_1-S_0 transitions afford slightly increasing contributions from the H-L pair

upon protonation, meaning that the strong stabilization of the LUMO is more clearly reflected in the emission energy of [**1a**,$2H^+$] than it is in the T_1-S_0 emission of [**2a**,H^+]. The emission remains quite intense with a similar quantum yield and lifetime (Φ = 8.2%, τ = 5.4 ns, Table S3). Similar g_{lum} values as for *P*- and *M*-**1a** were obtained for protonated samples (*P*-[**1a**,$2H^+$][BF_4^-]: $+3.2\times10^{-3}$ and *M*-[**1a**,$2H^+$][BF_4^-]: -2.5×10^{-3} at 590 nm). Overall, this significant λ_{em} change from the blue to yellow fluorescence (Figure 2c) accompanied by CPL enables us to consider this system as a reversible CPL-active pH-triggered on-off chiroptical switch at either 426 or 590 nm by successive addition of either "HBF_4" or Na_2CO_3/NEt_3 to acetone or CH_2Cl_2 solution of 3-(2-pyridyl)-4-aza[6]helicene **1a**. To the best of our knowledge, this is the first example of a helicene-based multi-responsive acid-base chiroptical switch.[14]

Conclusions

In conclusion, we have performed unprecedented pH-triggered switching of OR, CD and CPL activity using organic and organometallic helicene derivatives. The very large bathochromic shift of the emission observed upon protonation of azahelicene-bipy was theoretically rationalized by the decrease of aromaticity and stabilization of the LUMO level. Overall, this example illustrates the use of a chiral bipyridine ligand exhibiting "multiple personalities"[16] since it reveals original chiroptical and photophysical properties as well as *N*,*C* chelate behavior and it opens up new routes to chiral materials.

Experimental Section

Most experiments were performed using standard Schlenk techniques. Solvents were freshly distilled under argon from sodium/benzophenone (THF) or from phosphorus pentoxide (CH_2Cl_2). Starting materials were purchased from Aldrich. Column chromatography purifications were performed in air over silica gel (Merck Geduran 60, 0.063–0.200 mm). Irradiation reactions were conducted using a Heraeus TQ 700 mercury vapor lamp. NMR spectra ^1H, ^{13}C and ^{31}P were recorded at room temperature on a Bruker AV400 spectrometer equipped with a QNP switchable probe ^{13}C-^{31}P-^{19}F-^1H and operating at proton resonance frequency of 400 MHz. Chemical shifts are reported in parts per million (ppm) relative to Me_4Si as external standard. Assignment of proton atoms is based on COSY experiment.^{31}P NMR downfield chemical shifts are expressed with a positive sign, in ppm, relative to external 85% H_3PO_4. All spectra were obtained using deuterated dichloromethane or chloroform as solvents. The terms s, d, t, q, m indicate respectively singlet, doublet, triplet, quartet, multiplet; b is for broad and, dd is doublet of doublets, dt doublet of triplets, td triplet of doublets. Assignment of proton atoms is based on COSY, HMBC, HMQC experiments. Carbon atoms were assigned based on DEPT-135 experiments. Elemental analyses were performed by the CRMPO, University of Rennes 1. Specific rotations (in deg cm^2g^{-1}) were measured in a 1 dm thermostated quartz cell on a Perkin Elmer-341 polarimeter. Circular dichroism (in $M^{-1}cm^{-1}$) was measured on a Jasco J-815 Circular Dichroism Spectrometer (IFR140 facility - Biosit platform - Université de Rennes 1). UV/vis spectroscopy was conducted on a Varian Cary 5000 spectrometer. 2,2′-Bipyridine-6-carbaldehyde,[17,18] (benzo[c]phenanthren-3-ylmethyl)-triphenylphosphonium bromide[7] and *cis*-$(dmso)_2PtMe_2$[19] were prepared according to literature procedures.

Racemic 3-(2-pyridyl)-4-aza[6]helicene (±)-1a

1. A solution of (benzo[c]phenanthren-3-ylmethyl)triphenylphosphonium bromide[7] (1.465 g, 2.5 mmol) in 40 ml of anhydrous THF was placed in a Schlenk tube under argon and cooled to −78 °C for 5 minutes. To the stirred suspension *n*-BuLi (2.5 solution in hexanes, 1 ml, 26 mmol) was added dropwise. The reaction mixture turned deep red then warmed to room temperature slowly. After 45 minutes, the reaction mixture was cooled again to −78 °C, then 2,2′-bipyridine-6-carbaldehyde[17,18] (440 mg, 2.39 mmol) was added in one portion; the reaction mixture was warmed to room temperature and the color turned yellow white with stirring for 3 hours. The reaction mixture was filtered over celite and concentrated under vacuum, and the crude oily product was purified by column chromatography (silica gel, heptane/ethyl acetate 7:3) to give the olefine (*cis* and *trans* mixture) as a yellow solid (890 mg, 92%). ^{1}H NMR (300 MHz, CD_2Cl_2): δ 9.26 (1H, s), 9.20 (1H, d, J = 8.5 Hz), 9.17 (0.45H, s), 8.75 (1H, d, J = 3.6 Hz), 8.72 (0.5H, s), 8.65 (1.4H, d, J = 7.8 Hz), 8.33 (1.4H, t, J = 7.4 Hz), 8.15–7.73 (14.5H, m), 7.68 (2H, t, J = 7.8 Hz), 7.53 (1H, dd, J = 14.4, 7.3 Hz), 7.48–7.31 (4H, m), 7.28 (0.3H, s), 7.26–7.19 (0.4H, m), 7.16 (0.4H, d, J = 12.3 Hz), 6.93 (0.4H, d, J = 12.2 Hz). Elemental analysis, calcd. (%) for C30H20N2: C, 88.21; H, 4.93; N, 6.86; found C 87.98, H 4.85, N 6.80.

2. The mixture of *cis* and *trans* olefin 6-(2-(benzo[c]phenanthren-2-yl)vinyl)-2,2′-bipyridine (100 mg) in 1 L toluene/THF (9:1) was irradiated for 5 hrs in the presence of catalytic amount of iodine using a 700W mercury vapor lamp. Then the solvent was stripped off and the crude product was purified over silica gel (heptane/ethyl acetate 8:2) to give (±)-**1a** as a yellow solid (90 mg, 90%). ^{1}H NMR (400 MHz, CD_2Cl_2): δ 8.56 (1 H, m, $H^{3'}$), 8.49 – 8.53 (1H, m, $H^{6'}$), 8.14 (2 H, s), 7.94 – 8.03 (4 H, m), 7.90 (2H, s), 7.86 (1H, d, J = 8.9 Hz), 7.80 (1H, d, J = 8 Hz, H^{13}), 7.79–7.74 (m, 1H, $H^{4'}$), 7.65 (1 H, d, J = 8.7 Hz), 7.57 (d, J = 9 Hz, 1 H, H^{16}), 7.22 (1 H, ddd, J = 7.3, 4.8, 1.1 Hz, $H^{5'}$), 7.15 (1 H, ddd, J = 8, 6.9, 1.1 Hz, H^{14}), 6.64 (1 H, ddd, J = 8.5, 6.9, 1.4 Hz, 1 H, H^{15}). ^{13}C NMR (101 MHz, CD_2Cl_2): δ 156.33 (*C*), 154.86 (*C*), 149.45 (*C*H), 147.54 (*C*), 137.13 (*C*H), 135.94 (*C*H), 133.69 (*C*), 132.59 (*C*), 132.07 (*C*), 131.74 (*C*), 130.63 (*C*H), 129.88 (*C*), 129.81 (*C*H), 128.61 (*C*H), 128.31 (*C*H), 128.12 (*C*H), 128.04 (*C*H), 128.03 (*C*H), 127.97 (*C*), 127.60 (*C*H), 127.42 (*C*H), 126.54 (*C*H), 126.15 (*C*H), 125.77 (*C*), 125.58 (*C*H), 124.39 (*C*), 124.27 (*C*H), 121.54 (*C*H), 116.94 (*C*H). Elemental analysis, calcd. (%) for $C_{30}H_{18}N_2$: C, 88.64; H, 4.46; N, 6.89; found C 88.55, H 4.39, N 6.83.

3-Pyridinium-4-azonia[6]helicene [1a,2H$^+$][2BF$_4^-$]—Compound **1a** (10 mg, 0.024 mmol) was dissolved in 4 ml CH_2Cl_2 then $[H_2O.HBF_4]_2$[18C6][15] (0.027 mmol, 13 mg) was added and the reaction mixture was stirred for 2 hours at room temperature. CH_2Cl_2 was evaporated to small volume, and then ether was added to observe yellow precipitate that was filtrated and washed with ether to remove the excess acid. Finally, the precipitate was dried under vacuum to obtain [**1a**,2H$^+$][2BF$_4^-$] as yellow-orange powder (12.6 mg, 90%). ^{1}H NMR (300 MHz, CD_2Cl_2): δ 9.08 – 9.15 (1 H, m, $H^{6'}$), 8.47 – 8.59 (2 H, AB, J = 9.1 Hz), 8.34 – 8.43 (2 H, m), 8.27 (2 H, d, J = 8.3 Hz), 8.12 – 8.19 (3 H, m), 8.02 – 8.09 (2

H, m), 7.94 (1 H, dd, J = 8.10, 0.8 Hz, H^{13}), 7.88 (1 H, ddd, J = 7.6, 5.4, 1.1 Hz, $H^{5'}$), 7.65 (1 H, 6, J = 8.6 Hz, H^{16}), 7.47 (1 H, d, J = 9.0 Hz), 7.29 (1 H, ddd, J = 8, 6.9, 1.1 Hz, H^{14}), 6.83 (1 H, ddd, J = 8.5, 7.0, 1.4 Hz, H^{15}). ^{13}C NMR (75 MHz, CD_2Cl_2): δ 147.07 (*C*), 146.53 (*C*H), 144.34 (*C*H), 144.25 (*C*), 140.42 (*C*H), 135.39 (*C*H), 134.28 (*C*) 132.78 (*C*), 132.68 (*C*), 132.62 (*C*), 130.30 (1 *C*H), 129.19 (*C*H), 129.18 (*C*H), 129.06 (*C*), 128.68 (*C*H), 127.99 (*C*H), 127.70 (*C*H), 127.68 (*C*H), 127.56 (*C*H), 127.40 (*C*), 127.26 (*C*), 126.80 (*C*), 126.66 (*C*H), 126.61 (*C*H), 126.30 (*C*H), 125.81 (*C*H), 124.10 (*C*), 123.55 (*C*H), 116.10 (*C*H). *One C is missing.* Elemental analysis, calcd. (%) for $C_{30}H_{20}B_2F_8N_2$: C, 61.90; H, 3.46; N, 4.81; found C 62.63, H 3.56, N 4.57.

3-Pyridyl-4-aza[4]helicene 1b

1. A solution of 2-methylnaphtyltriphenylphosphonium bromide (433 mg, 0.89 mmol) in 15 ml of anhydrous THF was placed in a Schlenk tube under argon and cooled to −78 °C. To the stirred suspension *n*-BuLi (1.6N solution in hexanes, 0.58 ml, 0.93 mmol) was added dropwise. The reaction mixture turned deep red then warmed to room temperature slowly. After 45 minutes, the reaction mixture was cooled again to −78 °C. Then 2,2′-bipyridine-6-carbaldehyde[17,18] (157 mg, 0.85 mmol) was added in one portion; the reaction mixture was warmed to room temperature and the color turned yellow white with stirring overnight. The reaction mixture was filtered over celite and concentrated under vacuum, and the crude oily product was purified by column chromatography (silica gel, heptane/ethyl acetate 8:2) to give the olefin (*cis* and *trans* mixture) as a yellow solid (215 mg, 82%). ^{1}H NMR (400 MHz, $CDCl_3$): δ 8.63 (1 H, d, J = 4.0 Hz), 8.51 – 8.58 (2 H, m), 8.22 (1 H, d, J = 8.0 Hz), 8.14 (1 H, d, J = 8.0 Hz), 7.85 – 7.95 (3 H, m), 7.70 – 7.84 (7 H, m), 7.59 – 7.69 (2 H, m), 7.53 (1 H, t, J = 7.9 Hz), 7.34 – 7.48 (7 H, m), 7.23 – 7.34 (2 H, m), 7.11 – 7.17 (2 H, m), 6.96 (1 H, d, J = 12.3 Hz), 6.76 (1 H, d, J = 12.3 Hz). Elemental analysis, calcd. (%) for $C_{22}H_{16}N_2$: C, 85.69; H, 5.23; N, 9.08; found C 84.50, H 5.19, N 9.03.

2. The mixture of *cis* and *trans* olefin 6-(2-(benzo[c]phenanthren-2-yl)vinyl)-2,2′-bipyridine (500 mg) in 700 mL toluene/THF (9:1) was irradiated for 15 hrs in the presence of catalytic amount of iodine using a 150W mercury vapor lamp. Then the solvent was stripped off and the crude product was purified over silica gel (heptane/ethyl acetate; 9:1) to give **1b** as yellow solid (370 mg, 75%). ^{1}H NMR (400 MHz, $CDCl_3$): δ 9.41 (1 H, d, J = 9 Hz, H^1), 8.98 (1 H, d, J = 8.1 Hz, H^{12}), 8.59 – 8.68 (3 H, m, $H^{6'}$, $H^{2'}$, H^2), 8.00 – 8.12 (2H, AB, J = 8.7 Hz, H^5, H^6) 7.98 (1 H, dd, J = 7.9, 1.7 Hz, H^{12}), 7.78 – 7.89 (2 H, AB, J = 8.5 Hz, H^7,^{8}), 7.81 (1 H, m, $H^{4'}$), 7.63 – 7.69 (1 H, m, H^{11}), 7.56 – 7.62 (1 H, m, H^{10}), 7.29 (1 H, ddd, J = 7.4, 4.8, 1.3 Hz, $H^{5'}$). ^{13}C NMR (75 MHz, CD_2Cl_2): δ 156.46 (*C*), 155.23 (*C*), 149.67 (*C*H), 148.95 (*C*), 137.28 (*C*H), 136.67 (*C*H), 133.98 (*C*), 131.53 (*C*), 131.11 (*C*H), 130.56 (*C*), 129.43 (*C*H), 129.20 (*C*H), 128.67 (*C*H), 127.86 (*C*H), 127.31 (*C*), 127.15 (*C*H), 127.08 (*C*H), 126.75 (*C*H), 125.87 (*C*), 124.45 (*C*H), 121.80 (*C*H), 118.36 (*C*H). Elemental analysis, calcd. (%) for $C_{22}H_{14}N_2$: C, 86.25; H, 4.61; N, 9.14; found C 86.12, H 4.55, N 9.05.

Complex 2b—To a solution of *cis*-$(dmso)_2PtMe_2$[19] (20 mg, 0.05 mmol) in acetone (5 mL) was added 16 mg of proligand **1b** (0.05 mmol). The stirred solution was heated to 50° C and kept under a nitrogen atmosphere. After 5 h the mixture was cooled to room temperature, concentrated to small volume, and treated with pentane to form a precipitate. The solid was filtered off, washed with pentane, and vacuum-pumped to give the analytical sample 2b (27 mg, 90%) as an orange solid. ^{1}H NMR (400 MHz, CD_2Cl_2): δ 9.77 (1 H, d, $J_{H\text{-}H}$ = 6.0 Hz, $^3J_{Pt\text{-}H}$ = 12.1 Hz, $H^{6'}$), 9.54 (1 H, s, $^3J_{Pt\text{-}H}$ = 32 Hz, H^1), 9.04 (1 H, d, J = 8.5 Hz, H^{12}), 8.53 (1 H, d, J = 7.3 Hz, $H^{3'}$), 7.95 – 8.04 (3 H, m, $H^{5,4',9}$), 7.90 – 7.94 (1 H, m, H^6), 7.78–7.88 (2 H, AB, J = 8.5 Hz, $H^{7,8}$), 7.65 (1 H, t, J = 6.9 Hz, H^{11}), 7.58 (1 H, t, J = 7.3 Hz, H^{10}), 7.39 (1 H, t, J = 5.8 Hz, $H^{5'}$), 3.15 – 3.25 (6 H, s, $^3J_{Pt\text{-}H}$ = 18.4 Hz, H_{dmso}), 0.78 (3 H, s, $^2J_{Pt\text{-}H}$ = 83 Hz, $H_{Me\text{-}Pt}$). ^{13}C NMR (101 MHz, CD_2Cl_2): δ 164.75 (*C*), 161.97 (*C*), 150.64 (*C*H), 146.61 (*C*), 141.42 (*C*), 138.93 (*C*H), 138.56 (*C*H), 133.51 (*C*), 131.15 (*C*), 130.48 (*C*), 128.98 (*C*H), 128.75 (*C*H), 128.60 (*C*H), 128.08 (*C*H), 127.78 (*C*H), 127.02 (*C*), 126.72 (*C*H), 126.24 (*C*H), 126.09 (*C*), 125.98 (*C*H), 125.11 (*C*H), 122.13 (*C*H), 43.82 (2*C*H_3), −13.52 (*C*H_3). Elemental analysis, calcd. (%) for C25H22N2OPtS: C 50.58; H, 3.74; found C, 50.47, H 3.68.

Complex Pt(1b)Cl(dmso)—To a solution of **2b** (40 mg, 0.067 mmol) in 8 mL of acetone was added with vigorous stirring 0.34 mL of dmso and 0.67 mL of aqueous 0.1 M HCl (0.067 mmol). After 8 h the solution was concentrated to a small volume then extracted with CH_2Cl_2, dried with Na_2SO_4, and concentrated to a small volume. The residue was then treated with pentane to form a precipitate which was filtered, washed with pentane, and vacuum-pumped to give the analytical sample Pt(**1b**)Cl(dmso) (29 mg, 70%) as a yellow solid. ^{1}H NMR (400 MHz, CD_2Cl_2): δ 10.17 (1 H, s, $^3J_{Pt\text{-}H}$=25 Hz, H^1), 9.64 (1 H, d, J=6.0 Hz, $H^{6'}$), 9.13 (1 H, d, J=8.3 Hz, H^{12}), 8.46 (1 H, d, J=9.0 Hz, $H^{3'}$), 7.91 – 8.07 (4 H, m, $H^{5,6,4',9}$), 7.77 – 7.89 (2H, AB, J=8.5 Hz, $H^{7,8}$), 7.53 – 7.67 (2 H, m, $H^{10,11}$), 7.43 (1 H, t, J=6.0 Hz, $H^{5'}$), 3.62 (6 H, s, $^3J_{Pt\text{-}H}$=12 Hz, H_{dmso}). Elemental analysis, calcd. (%) for $C_{24}H_{19}ClN_2OPtS$: C, 46.95; H, 3.12; found C 46.78, H 3.01.

Complex 3b—To a solution of Pt(**1b**)Cl(dmso) (14.6 mg, 0.024 mmol) in CH_2Cl_2 (5 mL) was added 6.2 mg of PPh_3 (0.024 mmol). The stirred solution was kept under a nitrogen atmosphere. After 2 h the mixture was concentrated to small volume and treated with pentane to form a precipitate. The solid was filtered off, washed with pentane, and vacuum-pumped to give the analytical sample **3b** as a yellow solid (19 mg, 98%) that was crystallized with slow diffusion of pentane into CH_2Cl_2 solution. ^{1}H NMR (400 MHz, CD_2Cl_2): δ 9.86 (1 H, m, $H^{6'}$), 8.52 (1 H, d, J = 8.3 Hz, $H^{3'}$), 8.35 (1 H, s, $^3J_{Pt\text{-}H}$ = 56 Hz, H^1), 8.01 – 8.08 (1 H, m, $H^{4'}$), 7.89 (1 H, d, J = 9 Hz), 7.74 – 7.81 (6 H, m), 7.71 (1 H, d, J = 8.3 Hz, H^{12}), 7.66 (1 H, d, J = 8.8 Hz), 7.53 – 7.60 (2 H, m), 7.45 – 7.52 (1 H, m), 7.36 – 7.43 (1 H, m), 7.31 (1 H, ddd, J = 8.1, 6.9, 1 Hz, $H^{5'}$), 7.23 – 7.29 (3 H, m), 7.11 – 7.20 (6 H, m), 6.40 (1 H, ddd, J = 8.4, 7.0, 1.4 Hz, H^{11}). ^{13}C NMR (101 MHz, CD_2Cl_2): δ 163.27 (*C*H), 148.5 (*C*), 145.05 (*C*), 142.30 (*C*H), 140.12 (*C*H), 135.32 – 135.87 (6*C*H), 133.0 (*C*), 130.97 (*C*H), 130.96 (*C*H), 129.91 (*C*), 129.53 (*C*), 129.29 (*C*), 128.94 (*C*H), 128.79 (*C*H), 128.60 (*C*), 128.53 (*C*), 128.41 (*C*), 127.7 – 128.14 (9*C*H), 127.36 (*C*H), 126.56 (*C*), 126.35 (*C*H), 126.09 (*C*), 126.03 (*C*H), 125.44 (*C*H), 125.21 (*C*), 124.74 (*C*H), 122.14 (*C*H). ^{31}P

NMR (162 MHz, CD_2Cl_2) δ 22.70 ($J_{Pt\text{-}P}$ = 4301.5 Hz). Elemental analysis, calcd. (%) for $C_{40}H_{28}ClN_2PPt$: C, 60.19; H, 3.54; found C 60.03, H 3.45.

Complexes *P*- and *M*-2a—To a solution of *cis*-$(dmso)_2PtMe_2$[19] (20 mg, 0.05 mmol) in acetone (5 mL) was added 21.3 mg of *P*-**1a** (0.05 mmol). The stirred solution was heated to 50° C and kept under a nitrogen atmosphere. After 5 h the mixture was cooled to room temperature, concentrated to small volume, and treated with pentane to form a precipitate. The solid was filtered off, washed with pentane, and vacuum-pumped to give the analytical sample *P*-**2a** (31 mg, 90%) as an orange solid. The same procedure was used to prepare *M*-**2a** from *M*-**1a**. ^{1}H NMR (400 MHz CD_2Cl_2): δ 9.48 – 9.57 (1 H, m, $^3J_{Pt\text{-}H}$ = 20 Hz, H$^{6'}$), 8.36 – 8.41 (1 H, m), 8.10 (1 H, s, $^3J_{Pt\text{-}H}$ = 62.5 Hz), 7.98 (2 H, s), 7.80 – 7.96 (7 H, m), 7.72 (1 H, dd, *J* = 8.1, 1.40 Hz), 7.61 – 7.67 (1 H, m), 7.24 (1 H, ddd, *J* = 7.4, 5.6, 1.5 Hz), 7.13 (1 H, ddd, *J*=8, 6.9, 1.1 Hz), 6.63 (1 H, ddd, *J* = 8.5, 6.9, 1.4 Hz), 2.99 (3 H, s, $^3J_{Pt\text{-}H}$ = 18 Hz), 2.89 (3 H, s, $^3J_{Pt\text{-}H}$ = 18 Hz), −0.38 (3 H, s, $^2J_{Pt\text{-}H}$ = 83.3 Hz). ^{13}C NMR (101 MHz, CD_2Cl_2): δ 162.18 (C), 148.49 (*C*H), 150.80 (*C*H), 145.68 (C), 140.90 (C), 138.69 (*C*H), 138.41 (*C*H), 133.56 (C), 131.73 (C), 131.70 (C), 130.04 (C), 129.63 (*C*H), 128.80 (*C*H), 128.44 (*C*H), 128.42 (C), 128.23 (C), 128.16 (*C*H), 128.01 (*C*H), 127.80 (*C*H), 127.56 (*C*H), 127.50 (*C*H), 127.21 (C), 127.17 (*C*H), 126.41 (*C*H), 126.05 (*C*H), 126.03 (C), 125.28 (2*C*H), 124.62 (C), 122.24 (*C*H), 44.05 (*C*H$_3$), 43.88 (*C*H$_3$), −14.21 (*C*H$_3$). Elemental analysis, calcd. (%) for $C_{33}H_{26}N_2OPtS$: C, 57.13; H, 3.78; found C 57.05, H 3.72.

Complexes *P*- and *M*-[2a,H$^+$][BF$_4^-$]—To a solution of *P*-**2a** (5 mg, 7.2 μmol) in CH_2Cl_2 (2 mL) was added 3 mg of $[H_2O.HBF_4]_2[18C6]$[15] (2 mg, 4 μmol). After 2 h the mixture was concentrated to small volume and treated with Et_2O to form a precipitate. The solid was filtered off, washed with Et_2O, and vacuum pumped to give the analytical sample *P*-[**2a**,H$^+$][BF$_4^-$] (5.2 mg, 92%) as a bright-orange solid. The same procedure was used to prepare *M*-[**2a**,H$^+$][BF$_4^-$] from *M*-**2a**. ^{1}H NMR (400 MHz, CD_2Cl_2): δ 13.58 (1 H, br, N*H*), 9.87 (1 H, d, *J* = 5.5 Hz, $^3J_{Pt\text{-}H}$ = 20 Hz, H$^{6'}$), 9.00 (1 H, s, $^3J_{Pt\text{-}H}$ = 64.2 Hz, H^1), 8.79 (1 H, d, *J* = 7.8 Hz, H$^{3'}$), 8.52 (2 H, s), 8.21 – 8.33 (2 H, m), 8.06 – 8.17 (2 H, m), 7.95 – 8.05 (2 H, m), 7.88 (1 H, d, *J* = 7.5 Hz, H^{13}), 7.59 – 7.70 (2 H, m, H$^{5',16}$), 7.29 (1 H, m, H^{14}), 6.87 (1 H, m, H^{15}), 3.16 (3 H, s, $^3J_{Pt\text{-}H}$ = 21 Hz), 3.06 (3 H, s, $^3J_{Pt\text{-}H}$ = 21 Hz, H$_{dmso}$), −0.21 (3 H, s, $^3J_{Pt\text{-}H}$ = 82 Hz, H$_{Me\text{-}Pt}$). ^{13}C NMR (101 MHz, CD_2Cl_2): δ 152.03(*C*H), 146.98 (*C*H), 140.99 (*C*), 140.22 (*C*H), 136.03 (*C*), 135.53 (*C*H), 134.1 (*C*), 134.14 (*C*), 133.01 (*C*), 132.18 (*C*), 131.70 (*C*), 129.94 (*C*H), 129.11 (*C*H), 128.88 (*C*H), 128.31 (*C*), 128.15 (*C*H), 128.01 (*C*H), 127.92 (*C*H), 127.25 (*C*H), 127.20 (*C*), 127.11 (*C*H), 126.75 (*C*), 126.71 (*C*H), 126.23 (*C*H), 126.15 (*C*), 126.04 (*C*H), 125.88 (*C*), 123.59 (*C*), 123.43 (*C*H), 120.03 (*C*H), 43.76 (*C*H$_3$), 43.73 (*C*H$_3$), −13.81 (*C*H$_3$). Elemental analysis, calcd. (%) for $C_{33}H_{27}BF_4N_2OPtS$: C, 50.72; H, 3.48; N, 3.58; found C 50.83, H 3.53, N 3.49.

Supplementary Material

Refer to Web version on PubMed Central for supplementary material.

Acknowledgments

We thank the Ministère de l'Education Nationale, de la Recherche et de la Technologie, the Centre National de la Recherche Scientifique (CNRS), the ANR (12-BS07-0004-METALHEL-01 and ANR-10-BLAN-724-1-NCPCHEM) and the LIA CNRS Rennes-Durham (MMC) for financial support. G.M. thanks the National Institute of Health, Minority Biomedical Research Support (1 SC3 GM089589-04 and 3 S06 GM008192-27S1) and the Henry Dreyfus Teacher-Scholar Award for financial support, while K.K.D. thanks the NIH MARC Grant 2T34GM008253-26 for a research fellowship. J.A. acknowledges support from the National Science Foundation grant CHE-1265833 and the Center for Computational Research at the University at Buffalo for providing computational resources. M.S. is grateful from financial support from the Foundation for Polish Science Homing Plus programme co-financed by the European Regional Development Fund and the Ministry of Science and Higher Education in Poland 'Outstanding Young Scientist' scholarship.

References

1. a) Amabilino, D., editor. Chirality at the Nanoscale, Nanoparticles, Surfaces, Materials and more. Wiley-VCH; 2009. b) Feringa, BL.; Browne, WR., editors. Molecular Switches. 2. Wiley-VCH; 2011.
2. a) Shen Y, Chen C-F. Chem Rev. 2012; 112:1463–1535. [PubMed: 22017405] b) Gingras M. Chem Soc Rev. 2013; 42:1051–1095. [PubMed: 23151680] c) Bosson J, Gouin J, Lacour J. Chem Soc Rev. 2014; 43:2824–2840. [PubMed: 24500211] d) Saleh N, Shen C, Crassous J. Chem Sci. 2014; 5:3680–3694.
3. Selected examples of CPL active helicenes: Field JE, Muller G, Riehl JP, Venkataraman D. J Am Chem Soc. 2003; 125:11808–11809. [PubMed: 14505389] Sawada Y, Furumi S, Takai A, Takeuchi M, Noguchi K, Tanaka K. J Am Chem Soc. 2012; 134:4080–4083. [PubMed: 22335235] Phillips KES, Katz TJ, Jockusch S, Lovinger AJ, Turro NJ. J Am Chem Soc. 2001; 123:11899–11907. [PubMed: 11724596] Kaseyama T, Furumi S, Zhang X, Tanaka K, Takeuchi M. Angew Chem, Int Ed. 2011; 50:3684–3687.Shen C, Anger E, Srebro M, Vanthuyne N, Deol KK, Jefferson TD Jr, Muller G, Williams JAG, Toupet L, Roussel C, Autschbach J, Réau R, Crassous J. Chem Sci. 2014; 5:1915–1927. [PubMed: 24855556] Nakamura K, Furumi S, Takeuchi M, Shibuya T, Tanaka K. J Am Chem Soc. 2014; 136:5555–5558. [PubMed: 24670158]
4. a) Norel L, Rudolph M, Vanthuyne N, Williams JAG, Lescop C, Roussel C, Autschbach J, Crassous J, Réau R. Angew Chem Int Ed. 2010; 49:99–102.b) Anger E, Rudolph M, Norel L, Zrig S, Shen C, Vanthuyne N, Toupet L, Williams JAG, Roussel C, Autschbach J, Crassous J, Réau R. Chem Eur J. 2011; 17:14178–14198. [PubMed: 22052676] c) Anger E, Rudolph M, Shen C, Vanthuyne N, Toupet L, Roussel C, Autschbach J, Crassous J, Réau R. J Am Chem Soc. 2011; 133:3800–3803. [PubMed: 21348483] d) Shen C, Anger E, Srebro M, Vanthuyne N, Toupet L, Roussel C, Autschbach J, Réau R, Crassous J. Chem Eur J. 2013; 19:16722–16728. [PubMed: 24173674] e) Crespo O, Eguillor B, Esteruelas MA, Fernandez I, Garcia-Raboso J, Gomez-Gallego M, Martin-Ortiz M, Olivan M, Sierra MA. Chem Comm. 2012; 48:5328–5330. [PubMed: 22517029]
5. Maeda H, Bando Y. Pure Appl Chem. 2013; 85:1967–1978.Molecular Devices and Machines: A Journey into the Nanoworld. Balzani V, Venturi M, Credi A. Wiley2006Examples of CPL-active cyclo-iridiated complexes: Schaffner-Hamann C, von Zelewsky A, Barbieri A, Barigelletti F, Muller G, Riehl JP, Neels A. J Am Chem Soc. 2004; 126:9339–9348. [PubMed: 15281825] Walters RS, Kraml CM, Byrne N, Ho DM, Qin Q, Coughlin FJ, Bernhard S, Pascal RA Jr. J Am Chem Soc. 2008; 130:16435–16441. [PubMed: 18998648] Yang L, von Zelewsky A, Nguyen HP, Muller G, Labat G, Stoeckli-Evans H. Inorg Chim Acta. 2009; 362:3853–3856.Ashizawa M, Yang L, Kobayashi K, Sato H, Yamagishi A, Okuda F, Harada T, Kuroda R, Haga M. Dalton Trans. 2009:1700–1702. [PubMed: 19240900]
6.

For previous helicenes with bipyridine moieties see: Fox JM, Katz TJ. J Org Chem. 1999; 64:302–305. [PubMed: 11674120] Deshayes K, Broene RD, Chao I, Knobler CB, Diederich F. J Org Chem. 1991; 56:6787–6795.Takenaka N, Sarangthem RS, Captain B. Angew Chem Int Ed. 2008; 47:9708–9710.Chen J, Captain B, Takenaka N. Org Lett. 2011; 13:1654–1657. [PubMed: 21366250]

7. Lightner DA, Hefelfinger DT, Powers TW, Frank GW, Trueblood KN. J Am Chem Soc. 1972; 94:3492–3497.
8. a) Crassous J. Chem Soc Rev. 2009; 38:830–845. [PubMed: 19322474] b) Crassous J. Chem Comm. 2012; 48:9684–9692. [PubMed: 22617840] c) Zhou YH, Li J, Wu T, Zhao XP, Xu QL, Li X-L, Yu M-B, Wang LL, Sun P, Zheng YX. Inorg Chem Commun. 2013; 29:18–21.d) Kaes C, Katz A, Hosseini MW. Chem Rev. 2000; 100:3553–3590. [PubMed: 11749322]
9. a) Butschke B, Schwarz H. Chem Sci. 2012; 3:308–326.b) Moorlag C, Wolf MO, Bohne C, Patrick BO. J Am Chem Soc. 2005; 127:6382–6393. [PubMed: 15853346]
10. Selected examples: Minghetti G, Stoccoro S, Cinellu MA, Soro B, Zucca A. Organometallics. 2003; 22:4770–4777.Zucca A, Cordeschi D, Stoccoro S, Cinellu MA, Minghetti G, Chelucci G, Manassero M. Organometallics. 2011; 30:3064–3074.Zucca A, Cordeschi D, Maidich L, Pilo MI, Masolo E, Stoccoro S, Cinellu MA, Galli S. Inorg Chem. 2013; 52:7717–7731. [PubMed: 23768142] Petretto GL, Rourke JP, Maidich L, Stoccoro S, Cinellu MA, Minghetti G, Clarkson GJ, Zucca A. Organometallics. 2012; 31:2971–2977.Maidich L, Zuri G, Stoccoro S, Cinellu MA, Masia M, Zucca A. Organometallics. 2013; 32:438–448.
11. The same successive reactions achieved on proligand 1a resulted in a mixture of compounds, probably due to the steric hindrance of the helix and of the PPh_3 ligand.
12. Nakai Y, Mori T, Sato K, Inoue Y. J Phys Chem A. 2013; 117:5082–5092. [PubMed: 23688122] Napagoda M, Rulisek L, Jancarik A, Klivar J, Samal M, Stara IG, Stary I, Solinova V, Kasicka V, Svatos A. Chem Plus Chem. 2013; 78:937. and references therein; Latterini L, Galletti E, Passeri R, Barbafina A, Urbanelli L, Emiliani C, Elisei F, Fontana F, Mele A, Caronna T. J Photochem Photobio A: Chem. 2011; 222:307–313.Alkorta I, Elguero J, Roussel C. Comput Theor Chem. 2011; 966:334–339.
13. a) Anger E, Srebro M, Vanthuyne N, Toupet L, Rigaut S, Roussel C, Autschbach J, Crassous J, Réau R. J Am Chem Soc. 2012; 134:15628–15631. [PubMed: 22715962] b) Graule S, Rudolph M, Vanthuyne N, Autschbach J, Roussel C, Crassous J, Réau R. J Am Chem Soc. 2009; 131:3183–3185. [PubMed: 19215079] c) Graule S, Rudolph M, Shen W, Lescop C, Williams JAG, Autschbach J, Crassous J, Réau R. Chem Eur J. 2010; 16:5976–6005. [PubMed: 20397244] d) Mendola D, Saleh N, Vanthuyne N, Roussel C, Toupet L, Castiglione F, Caronna T, Mele A, Crassous J. Angew Chem Int Ed. 2014; 53:5786–5790.
14. For an example of acid-base ECD switch see: Anger E, Srebro M, Vanthuyne N, Roussel C, Toupet L, Autschbach J, Réau R, Crassous J. Chem Comm. 2014; 50:2854–2856. [PubMed: 24322581] For an example of chemical-stimuli CPL switch see: Maeda H, Bando Y, Shimomura K, Yamada I, Naito M, Nobusawa K, Tsumatori H, Kawai T. J Am Chem Soc. 2011; 133:9266–9269. [PubMed: 21599014]
15. Atwood JL, Alvanipour A, Zhang H. J Cryst Spectrosc Res. 1992; 22:349–352.
16. Crabtree RH. Science. 2010; 330:455–456. [PubMed: 20966237]
17. Fang Y-Q, Hanan GS. Synlett. 2003; 6:852–854.
18. Ramírez-Monroy A, Swager TM. Organometallics. 2011; 30:2464–2467.

19. Appleton TG, Hall JR, Williams MA. J Organomet Chem. 1986; 303:139–149.

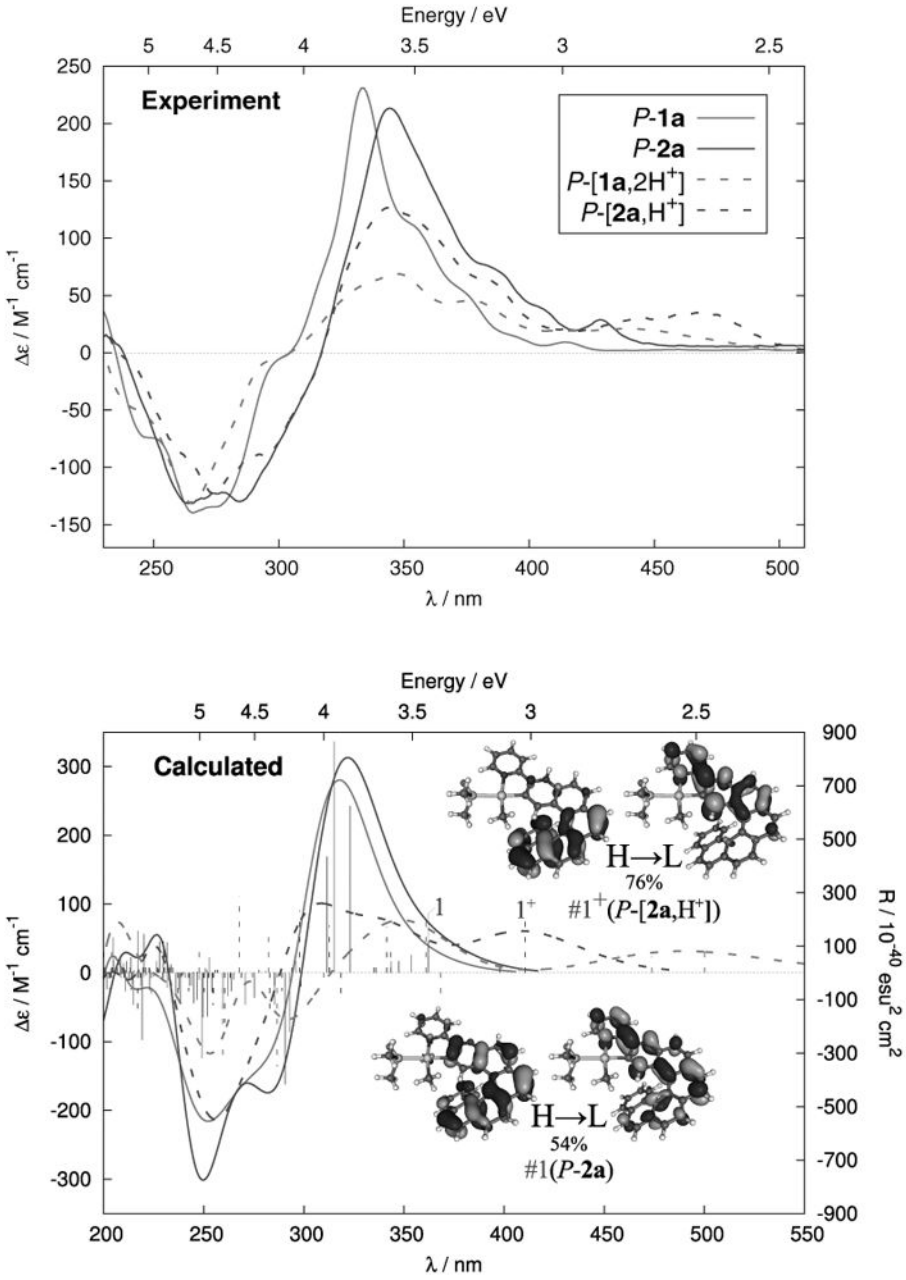

Figure 1.

Measured (up, CH_2Cl_2, ~10^{-5} M) and calculated (bottom) BHLYP CD spectra of proligand *P*-**1a** (plain grey), *P*-[**1a**,$2H^+$][$2BF_4^-$] (dotted grey), and of complexes *P*-**2a** (plain black) *P*-[**2a**,H^+][BF_4^-] (dotted black). Frontier MOs (0.03 au) of *P*-**2a** and *P*-[**2a**,H^+]. For assignments of the spectra see the SI.

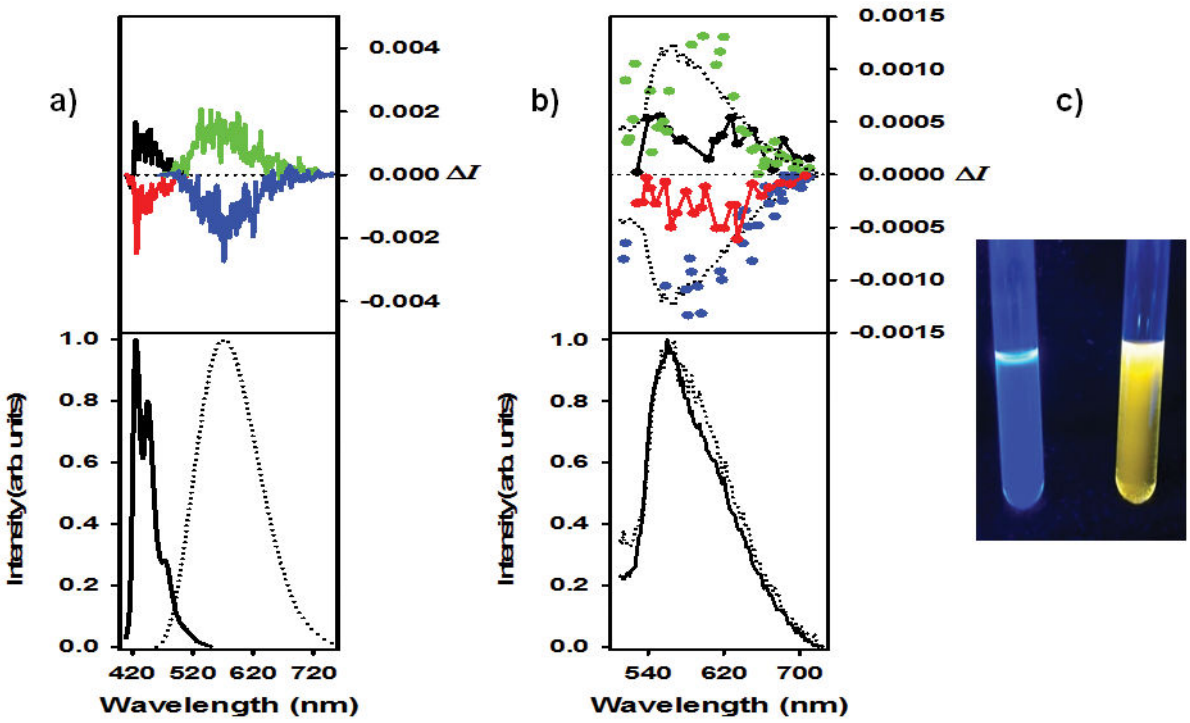

Figure 2.

a) CPL (top) and total emission (bottom) of fluorescent 3-(2-pyridyl)-4-aza[6]helicene *P*-**1a** (black), and *M*-**1a** (red) enantiomers to respectively *P*-[**1a**,2H$^+$][2BF$_4^-$] (green) and *M*-[**1a**, 2H$^+$][2BF$_4^-$] (blue), at 426 nm and at 590 nm respectively, in CH_2Cl_2 at r.t.; b) CPL (top) and total emission (bottom) of phosphorescent complex *P*-**2a** (black), and *M*-**2a** (red) enantiomers to respectively *P*-[**2a**,H$^+$][BF$_4^-$] (green) and *M*-[**2a**,H$^+$][BF$_4^-$] (blue), at 547 nm and at 555 nm respectively, in acetone at r.t. c) visual acid-base fluorescence switching of **1a**.

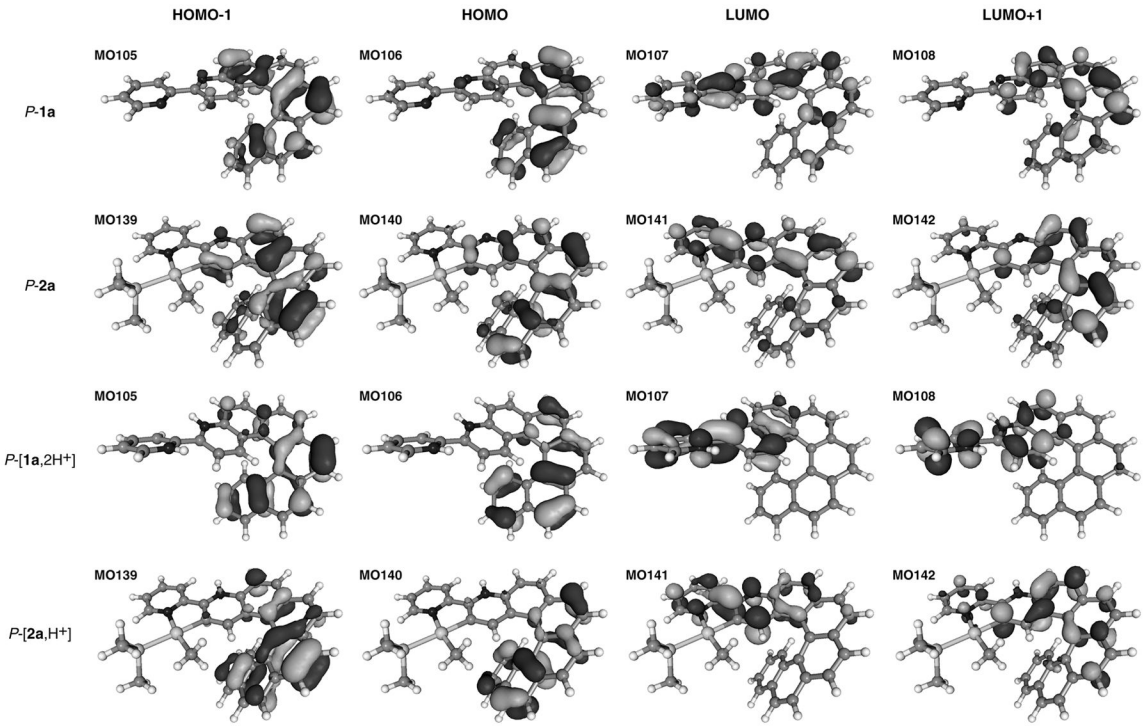

Figure 3.
Isosurfaces (0.04 au) of selected MOs of **1a**, [**1a**,$2H^+$] and **2a**, [**2a**,H^+].

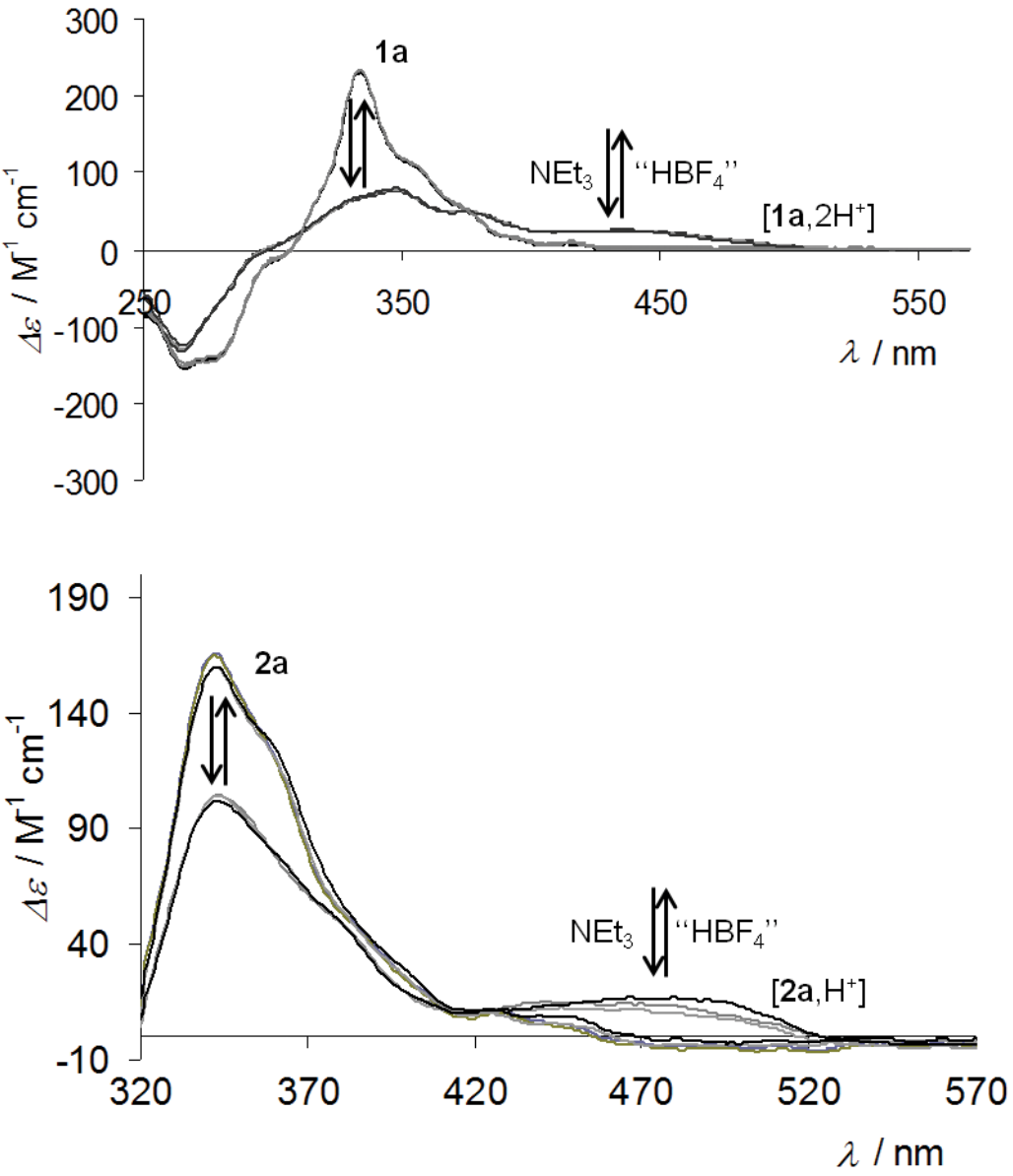

Figure 4.

Reversibility of the acid/base switching process by ECD spectroscopy for ligand **1a** (top) and complex **2a** (bottom) after several successive stoechiomeric addings of acid and base.

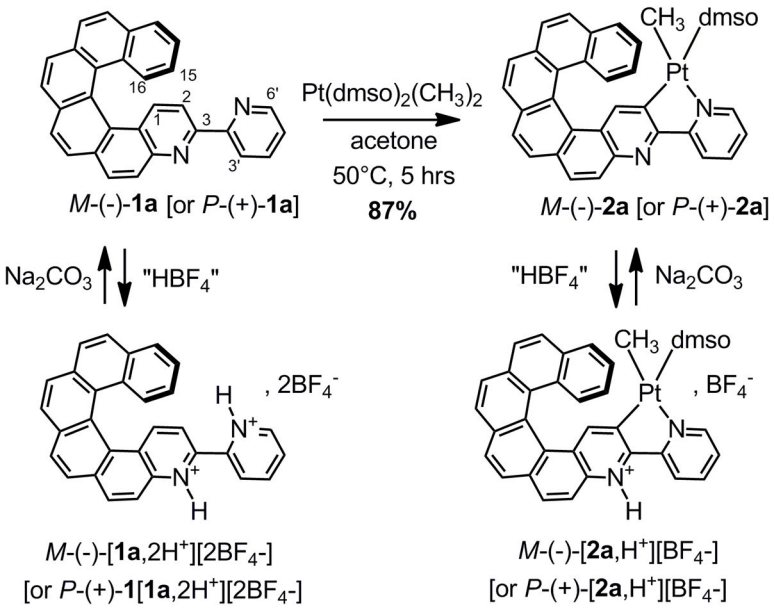

Scheme 1.

Synthesis of enantiopure rollover cycloplatinated Pt(CH_3)(dmso)(bipy - H) complexes *M*-(−)- and *P*-(+)-**2a** from enantiopure helicene-bipy proligands *M*-(−)- and *P*-(+)-**1a**. Reversible protonation/deprotonation in acetone.

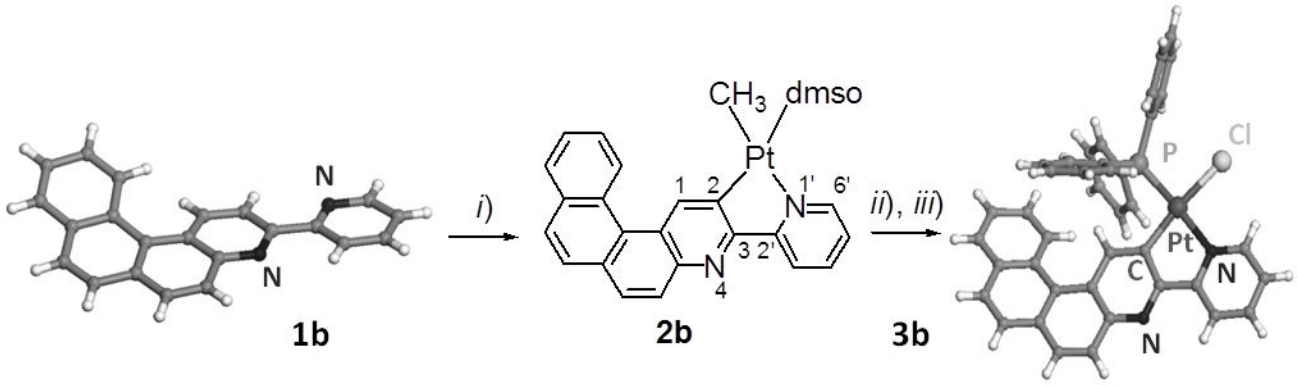

Scheme 2.

Reactivity of rollover cycloplatinated $Pt(CH_3)(dmso)(bipy - H)$ complex **2b**. *i*) $Pt(dmso)_2(CH_3)_2$, acetone, 50°C, 5 hrs, 89%. *ii*) HCl (0.1N), acetone, dmso, 8 hrs, 70%; *iii*) PPh_3, CH_2Cl_2, 2 hrs, 98%. X-ray crystallographic structures of proligand **1b** and of cycloplatinated complex **3b**.

Table 1

Experimental and calculated emission data of ligand species **1a** and [**1a**,2H$^+$] and of cycloplatinated complexes **2a** and [**2a**,H$^+$]. Energies, in eV. Oscillator strength/rotatory strength values in 10^{-40} cgs are listed in parentheses.

	***P*-1a**	***P*-[1a,2H$^+$]-#** [a]		***P*-2a**	***P*-[2a,H$^+$]**
		1	**2**		
Expt. [b]					
298 K	2.94, 2.79, 2.62	2.10		2.27, 2.12	2.23, 2.10
77 K	F: 2.97, 2.81, 2.63 P: 2.33, 2.15, 1.99	F: 3.13, 2.98, 2.81, 2.63 [g] P: 2.34, 2.15, 2.00 [g]		2.31, 2.13, 1.95	2.29, 2.10, 1.94 [g]
Calc. BHLYP/SV(P) [c]					
$S_1^{\{TDDFT\}}$ [d]	2.99 (0.4642/427.88)	1.86 (0.1631/174.24)	1.87 (0.1741/194.33)	2.94 (0.5507/459.99)	2.66 (0.3444/268.69)
$T_1^{\{TDDFT\}}$ [e]	2.18	1.49	1.50	2.16	2.08
$T_1^{\{DFT\}}$ [f]	2.08	1.60	1.61	2.06	2.08

[a] Conformer #1: dihedral angle N-C-C′-N′ of −150.0°, −170.5°, −175.7°, and −170.9° for S_0 ground state, S_1 excited state, T_1 excited state, and triplet configuration, respectively. Conformer #2: dihedral angle N-C-C′-N′ of 151.0°, 171.5°, 172.2°, and 168.7° for S_0 ground state, S_1 excited state, T_1 excited state, and triplet configuration, respectively.

[b] 298 K: DCM/acetone data for ligand/cycloplatinated species, 77 K: recorded in diethyl ether/isopentane/ethanol. F = fluorescence. P = phosphorescence.

[c] DCM/acetone calculations for ligand/cycloplatinated species.

[d] TDDFT S_1-S_0 energy difference at TDDFT BHLYP/SV(P) optimized S_1 geometry. In parentheses oscillator strength/rotatory strength values in 10^{-40} cgs are listed. To convert to integrated CPL intensity, in cgs units of power output per molecule, the following expression can be used: $\Delta I = 1.60041320 \cdot 10^{37} \cdot R_{cgs} \cdot E_{cgs4}$.

[e] TDDFT T_1-S_0 energy difference at TDDFT BHLYP/SV(P) optimized T_1 geometry.

[f] TDDFT T_1-S_0 energy difference at DFT BP/SV(P) optimized triplet configuration.

[g] At 77K, the equilibrium $B+H^+ \rightleftarrows BH^+$ is frozen.

Table 2

HOMO-to-LUMO character (in %) of S_0-S_1 absorption along with S_1-S_0 and T_1-S_0 emission transitions for ligand species **1a** and [**1a**,$2H^+$] and of cycloplatinated complexes **2a** and [**2a**,H^+]. BHLYP/SV(P) calculations with continuum solvent model for DCM.

	S_0-S_1	S_1-S_0	T_1-S_0
P-**1a**	33.0	93.7	72.3
P-[**1a**,$2H^+$] [a]	91.7	96.5	76.0
		96.4	75.9
P-**2a**	53.8	92.3	68.9
P-[**2a**,H^+]	75.5	90.1	61.6

[a] Results for two conformers are listed in the case of S_1 and T_1 excited states of *P*-[**1a**,$2H^+$], compare Table 1 (conformer #1 and #2).